Human Molecular Genetics, 2010, Vol. 19, No. 16 **3254–3265**
doi:10.1093/hmg/ddq234
Advance Access published on June 10, 2010

Mutant HSPB8 causes motor neuron-specific neurite degeneration

Joy Irobi[1,3], Leonardo Almeida-Souza[1,3], Bob Asselbergh[1,3], Vicky De Winter[1,3], Sofie Goethals[1,3], Ines Dierick[1,3], Jyothsna Krishnan[4], Jean-Pierre Timmermans[5], Wim Robberecht[4], Peter De Jonghe[2,3,6], Ludo Van Den Bosch[4], Sophie Janssens[1,3] and Vincent Timmerman[1,3,*]

[1]Peripheral Neuropathy and [2]Neurogenetics Groups, VIB Department of Molecular Genetics, University of Antwerp, Antwerp, Belgium, [3]Neurogenetics Laboratory, Institute Born-Bunge, University of Antwerp, Antwerp, Belgium, [4]Laboratory of Neurobiology and Experimental Neurology, Vesalius Research Center, VIB, University of Leuven, Leuven, Belgium, [5]Laboratory of Cell Biology and Histology, Department of Veterinary Sciences, University of Antwerp, Antwerp, Belgium and [6]Division of Neurology, University Hospital of Antwerp, Belgium

Received April 5, 2010; Revised and Accepted June 6, 2010

Missense mutations (K141N and K141E) in the α-crystallin domain of the small heat shock protein HSPB8 (HSP22) cause distal hereditary motor neuropathy (distal HMN) or Charcot-Marie-Tooth neuropathy type 2L (CMT2L). The mechanism through which mutant HSPB8 leads to a specific motor neuron disease phenotype is currently unknown. To address this question, we compared the effect of mutant HSPB8 in primary neuronal and glial cell cultures. In motor neurons, expression of both HSPB8 K141N and K141E mutations clearly resulted in neurite degeneration, as manifested by a reduction in number of neurites per cell, as well as in a reduction in average length of the neurites. Furthermore, expression of the K141E (and to a lesser extent, K141N) mutation also induced spheroids in the neurites. We did not detect any signs of apoptosis in motor neurons, showing that mutant HSPB8 resulted in neurite degeneration without inducing neuronal death. While overt in motor neurons, these phenotypes were only very mildly present in sensory neurons and completely absent in cortical neurons. Also glial cells did not show an altered phenotype upon expression of mutant HSPB8. These findings show that despite the ubiquitous presence of HSPB8, only motor neurons appear to be affected by the K141N and K141E mutations which explain the predominant motor neuron phenotype in distal HMN and CMT2L.

INTRODUCTION

Small heat shock proteins (sHSPs) are ubiquitously expressed conserved stress proteins involved in multiple cellular processes (1,2). These stress-induced molecular chaperones are vital for cell viability since they protect cells against environmental stress during aging, by assisting in the correct folding of denatured proteins, and by preventing aggregation of misfolded proteins (3).

Dominant missense mutations in two sHSPs genes, *HSPB8* (*HSP22*) and *HSPB1* (*HSP27*), have been associated with distal hereditary motor neuropathy (distal HMN MIM#158590) and Charcot-Marie-Tooth type 2 disease (CMT2L and CMT2F MIM#158590) (4–6). These neuropathies are clinically and genetically heterogeneous disorders of the peripheral nervous system (7). In distal HMN, the motor nerves are predominantly affected (8), although minor sensory abnormalities have been described in some families (9–11), explaining the clinical overlap between distal HMN and CMT2.

We previously reported that missense mutations (K141N and K141E) in the α-crystallin domain of HSPB8 play an important role in neurodegenerative disorders (5). Our

*To whom correspondence should be addressed at: VIB, Department of Molecular Genetics, University of Antwerp—CDE, Universiteitsplein 1, Building V, 2610 Antwerpen, Belgium. Tel: +32 32651024; Fax: +32 32651012; Email: vincent.timmerman@molgen.vib-ua.be

previous experiments showed that upon transient overexpression mutant HSPB8 formed cytoplasmic protein accumulations, which could sequester other soluble proteins including HSPB1. We also reported that mutant HSPB8 showed greater binding to the molecular partner HSPB1. Finally, we speculated that heat shock proteins could be involved in the formation of the stable neurofilament network and demonstrated that mutant HSPB1 altered neurofilament assembly (6). We hypothesize that despite the ubiquitous presence and pleiotropic functions of sHSP, there could be a motor neuron-specific pathway which would explain the predominant motor neuron phenotype observed in the distal HMN patients.

Since all previous studies were done in continuous cell lines, which might behave very different from primary cells, we decided to extend our previous results and examined the effect of mutant HSPB8 protein (K141N and K141E) in primary glial cells, in peripheral neurons including motor neuron and dorsal root ganglia (DRG) sensory neuron cultures and in cortical neurons. We found that mutations in HSPB8 strongly affect neurite length and integrity in motor neurons, whereas the other cell types were generally unaffected. Furthermore, degeneration of neurites in motor neurons seemed to occur independently of apoptosis and death of the cell body.

These results support the clinical descriptions of distal HMN type II with predominant involvement of motor neurons implying that mutant HSPB8 causes specific defects in preserving motor neuron axons. Furthermore, this study provides the first evidence that mutant HSPB8 induces neurite degeneration, which is a sign of axonal neuropathy.

RESULTS

Expression of mutant HSPB8 in primary motor neurons induces spheroids and shortened neurites

To find out if mutations in HSPB8 affect motor neuron viability, we studied the expression of the HSPB8 mutations (K141N and K141E) in primary motor neurons isolated from spinal cords of Wistar rat embryos. To this end, we used a highly efficient lentiviral approach which results in stable integration of the exogenous construct. Both wild-type (WT) and mutant HSPB8 constructs were transduced with similar efficiencies, yielding highly comparable protein expression levels (Supplementary Material, Fig. S1A). Furthermore, WT and mutant HSPB8-GFP fusion proteins showed a similar localization pattern within the motor neuron with homogenous distribution in cell body, nucleus and neurites (Supplementary Material, Fig. S1A). No aggregates could be detected in motor neurons, which was clearly distinct from earlier studies using transient transfection approaches (5).

Interestingly, striking differences could be observed when we compared the morphology of motor neurons transduced with WT-HSPB8 with those expressing mutant HSPB8, as judged by SMI32 neurofilament immunostaining. Motor neurons transduced with mutant HSPB8 clearly showed neurites with signs of degeneration, while this was not the case in neurons transduced with WT HSPB8 or control constructs (Fig. 1A–E). In cells expressing the K141N-HSPB8-GFP construct, we observed a reduction in length of the distal neurites (defined as shortened neurites in Materials and Methods) in ~80% of the mutant expressing motor neurons (data obtained at 4 days after transduction and for three independent experiments; percentage motor neurons in culture showing shortened neurites: GFP = 17.0 ± 1.0%, $n = 361$; WT-HSPB8-GFP = 14.0 ± 2.0%, $n = 192$; K141N-GFP = 86.0 ± 3.0%, $n = 150$, P-value = 2.5×10^{-5} and K141E-GFP = 75.0 ± 3.0%, $n = 300$, P-value = 8.7×10^{-6}) (Fig. 1F). In cells expressing the K141E-HSPB8-GFP construct, we observed a more severe phenotype consisting of shortened neurites, as well as neurites containing beaded-like structures resembling spheroids (data of three independent experiments, percentage of motor neurons showing beaded phenotype at day *in vitro* 7 (DIV7): GFP = 12.0 ± 5.0%, $n = 338$; WT-HSPB8-GFP = 0.0 ± 0.0%, $n = 192$; K141N-HSPB8-GFP = 9.0 ± 6.0%, $n = 150$, P-value = 0.1333 and K141E-HSPB8-GFP = 90.0 ± 1.0%, $n = 300$, P-value = 4.1×10^{-5}) (Fig. 1G).

To further investigate the integrity of motor neurons expressing HSPB8, we performed extensive quantifications measuring neurite length and number. Figure 1H illustrates the distribution of neurite length in different motor neurons. The mean neurite length of non-transduced motor neurons and motor neurons expressing either WT-HSPB8-GFP or native GFP protein was over 800 μm per soma, while the mean neurite length of motor neurons expressing either K141N or K141E-HSPB8-GFP protein was significantly lower, i.e. below 350 μm (non-transfected = 824 ± 332 μm, $n = 55$; GFP = 804 ± 325 μm, $n = 74$; WT-HSPB8-GFP = 939 ± 513 μm, $n = 61$; K141N-HSPB8-GFP = 233 ± 186 μm, $n = 30$, P-value = 1.2×10^{-10} and K141E-HSPB8-GFP = 338 ± 177 μm, $n = 47$, P-value = 8.4×10^{-12}). The average neurite number per motor neuron expressing WT-HSPB8-GFP was higher than four neurites per soma, whereas the average neurite number per motor neuron expressing either K141N or K141E-HSPB8-GFP protein was lower than three neurites per soma (GFP = 4.5 ± 1.5, $n = 248$; WT-HSPB8-GFP = 4.0 ± 1.5, $n = 219$; K141N-HSPB8-GFP = 1.6 ± 1.2, $n = 428$, P-value = 1.3×10^{-57} and K141E-HSPB8-GFP = 1.1 ± 0.9, $n = 424$, P-value = 4.5×10^{-74}) (Fig. 1I).

These data show that the expression of K141N/K141E-HSPB8 mutant protein strongly affects neurite integrity, compared with the WT, resulting in a higher percentage of motor neurons with neurite abnormalities.

Accumulation of amyloid precursor protein (APP) in neurites of mutant HSPB8 expressing motor neurons is a sign of neurite degeneration

To further verify if the neurite degeneration phenotype that we observed in motor neuron could be a sign of axonal degeneration, we used amyloid precursor protein (APP) as a marker for neurodegeneration. Early studies identified APP as a kinesin-binding protein (12,13). APP is a normal component of neurons transported by fast axonal transport, and specifically accumulates to detectable levels at sites where the cytoskeleton breaks down and therefore can be used as a read-out to study axonal transport defects (14–16). In healthy neuronal cells with normal axonal transport rates, APP is rapidly transported, leading to disperse signals on APP immunostainings. In cells

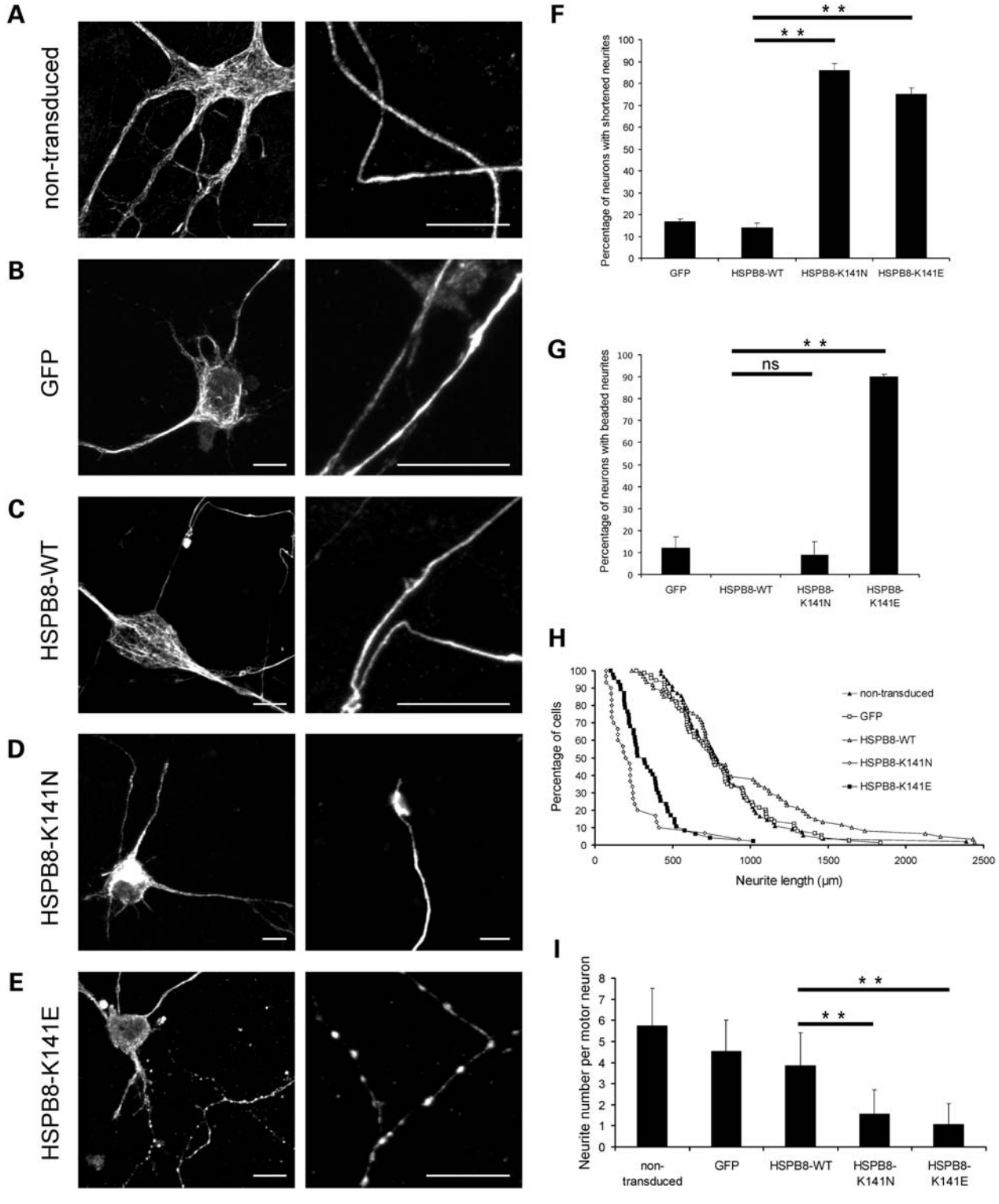

Figure 1. Mutant HSPB8 induces neurite abnormalities in primary motor neurons. Rat motor neurons were transduced with pLenti-GFP, pLenti-WT-HSPB8-GFP or mutant pLenti-K141N/K141E-HSPB8-GFP constructs at day *in vitro* 3 (DIV3) and immunostained against the non-phosphorylated epitope in neurofilament H (SMI32 antibody) at DIV7. Non-transduced motor neurons (**A**), motor neurons expressing native GFP (**B**) and WT-HSPB8 (**C**) show a punctate and homogenous neurofilament distribution in the motor neuron soma and normal formation of long and intact neurites, while neuritic processes of motor neurons expressing mutant HSPB8-K141N are shortened (**D**), and motor neurons expressing mutant HSPB8-K141E exhibited clear signs of neurite degeneration (spheroids or beaded neurites) (**E**). Scale bar = 10 μm. The incidence of neurite abnormalities in the motor neuron cultures were quantified by counting the proportion of neurons with abnormal (reduced or shortened) neurites (**F**) and with clear signs of neurite degeneration (beaded neurites) (**G**), by measuring neurite length distribution (**H**) and by counting the number of neurites per neuron (**I**). ns = not significant, $^{**}P$-value < 0.01.

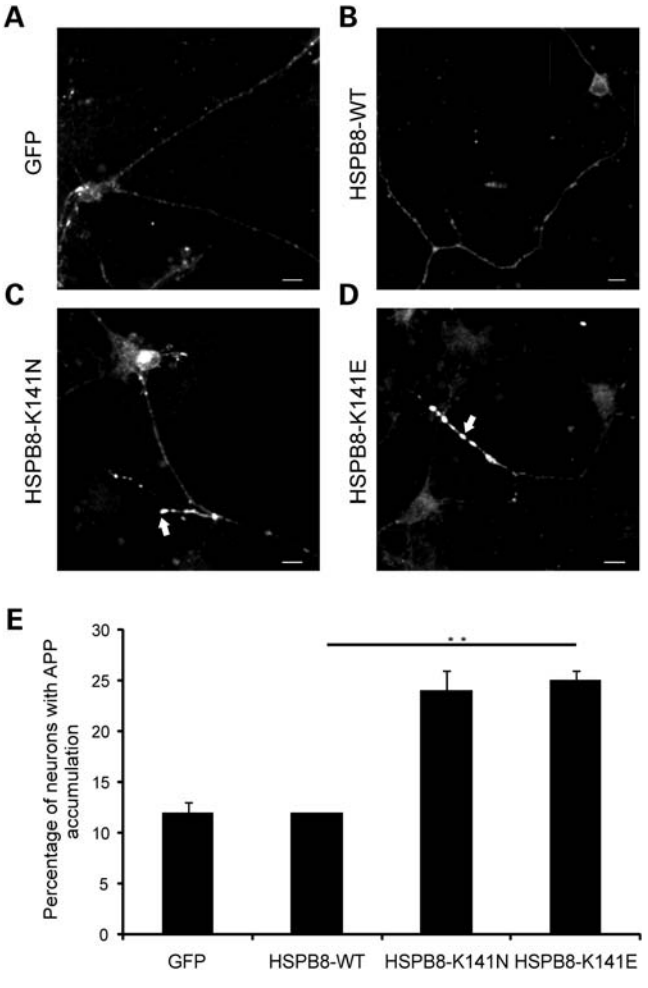

Figure 2. Motor neurons expressing mutant HSPB8 show enhanced neuritic APP accumulation. Rat motor neurons were transduced with pLenti-GFP, pLenti-WT-HSPB8-GFP or mutant pLenti-K141N/K141E-HSPB8-GFP constructs at DIV3 and immunostained using amyloid precursor protein (APP) antibody at DIV7. Motor neuron neurites expressing GFP (**A**) or HSPB8-WT (**B**) mainly show a faint and punctate appearance of APP in the neurites, similar to non-transduced neurites, while neurites of motor neuron expressing HSPB8-K141N (**C**) or HSPB8-K141E (**D**) accumulate more APP (arrow). The incidence of APP accumulation was quantified by counting the proportion of cells with strong neuritic APP accumulation (**E**). $^{**}P$-value < 0.01. Scale bar $= 10$ μm.

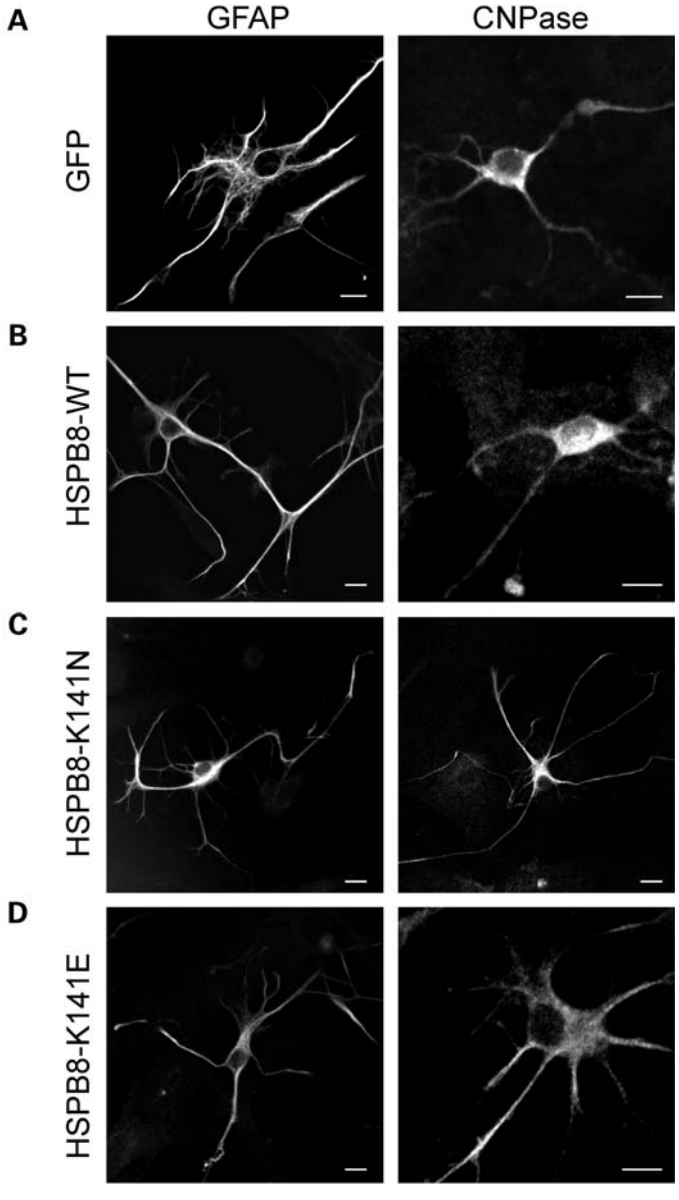

Figure 3. Expression of mutant HSPB8 has no detectable effect on the morphology of primary glial cells. Rat glial cells were transduced with pLenti-GFP, pLenti-WT-HSPB8-GFP or mutant pLenti-K141N/K141E-HSPB8-GFP constructs at DIV3 and immunostained at DIV7 with antibodies against either GFAP (left) or 2′, 3′-cyclic nucleotide 3′-phosphodiesterase (CNPase, right). The glial cells expressing GFP (**A**), WT-HSPB8 (**B**), mutant HSPB8-K141N (**C**) or HSPB8-K141E (**D**) were morphologically similar. Scale bar $= 10$ μm.

with axonal transport defects, APP rapidly accumulates leading to a strong signal in immunostainings. It is well established that defects in axonal transport and neurite degeneration are strongly linked (17) and therefore we examined this by immunostaining APP in neurites of motor neurons expressing either WT or mutant HSPB8 (Fig. 2A and B). Motor neurons expressing HSPB8-WT showed mostly a faint and punctate pattern of APP immunostaining indicative of a normal axonal transport, while strong accumulation of APP was detected in many neurites of mutant HSPB8 expressing motor neurons (data of three independent experiments at DIV7: GFP $= 12 \pm 1.0\%$, $n = 994$; WT-HSPB8-GFP $= 12 \pm 0.0\%$, $n = 971$; K141N-GFP $= 24.5 \pm 2.0\%$, $n = 864$, P-value $= 0.0082$ and K141E-GFP $= 25 \pm 1.0\%$, $n = 1029$, P-value $= 0.0019$) (Fig. 2C–E). These data therefore suggest that axonal transport blockage could be implicated in the development of mutant HSPB8 associated neurite degeneration.

Expression of mutant HSPB8 does not induce overt spheroids in neurites of primary sensory or cortical neurons or in glial cells

To check whether the phenotype we observed in primary motor neurons was cell type specific, we investigated if other cell types both of non-neuronal and neuronal origin,

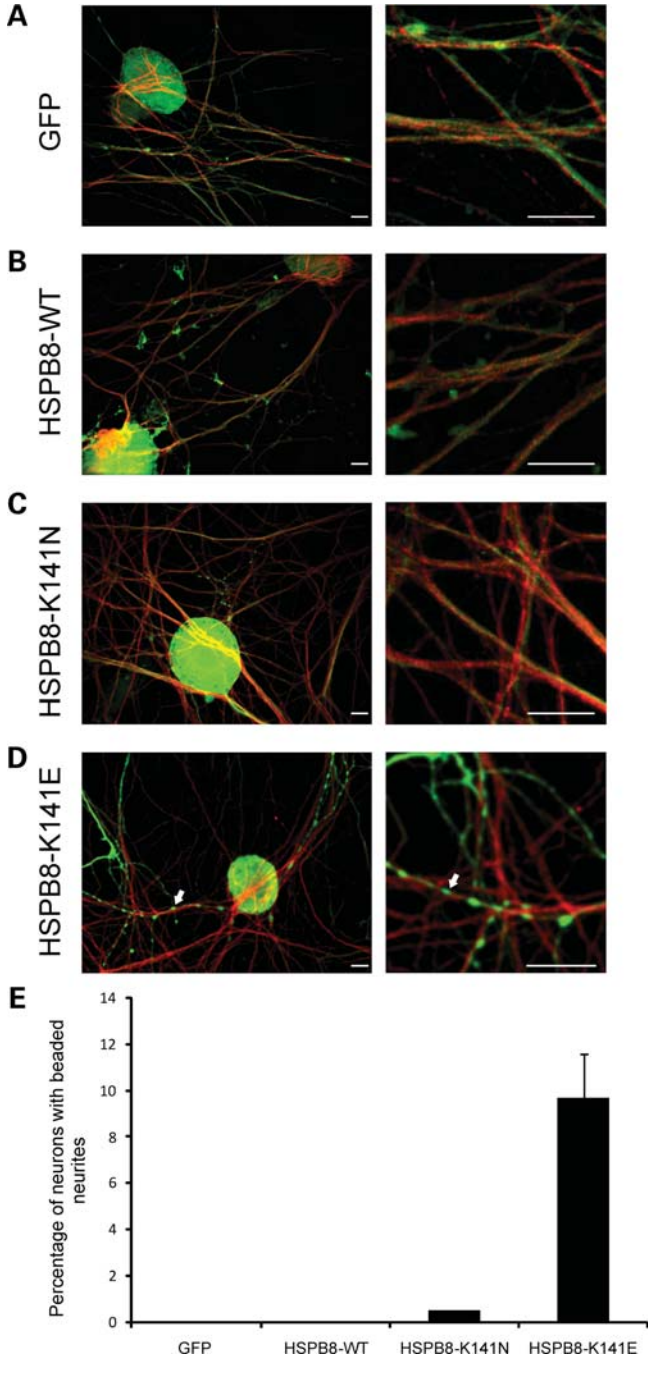

Figure 4. Mutant HSPB8 induces neurite degeneration in a small proportion of primary sensory neurons. Mouse sensory neurons were transduced with pLenti-GFP, pLenti-WT-HSPB8-GFP or mutant pLenti-K141N/K141E-HSPB8-GFP constructs at DIV6 and immunostained at DIV10 using β-III tubulin antibody. Merged confocal micrographs of GFP (green) and β-III tubulin (red) are shown (**A**–**D**). No signs of neurite degeneration were found in sensory neurons expressing GFP (A), HSPB8-WT (B) and HSPB8-K141N (C), while the neurites of some cells expressing HSPB8-K141E were clearly beaded (arrow) (D). Scale bar = 10 μm. The incidence of neurite degeneration was quantified by counting the proportion of neurons with beaded neurites (**E**). $^{**}P$-value < 0.01.

expressing mutant HSPB8, also exhibited signs of degeneration. To this end, we first expressed mutant and WT-HSPB8 in primary glial cells isolated from spinal cords of Wistar rat embryos. Similarly to neurons, glial cells appeared to be highly efficiently transduced by lentivirus yielding similar protein expression levels for WT and mutant constructs (Supplementary Material, Fig. S1B). Of note is that some glial cells overexpressing mutant HSPB8 constructs showed protein aggregates in the cytoplasm, probably due to higher expression levels compared with motor neurons.

However, despite these high expression levels, no gross morphological differences were detected between WT and mutant HSPB8 expressing cells, as judged by immunostainings with glial fibrillary acidic protein (GFAP) or 2′, 3′-cyclic nucleotide 3′-phosphodiesterase (CNPase) antibodies (Fig. 3A–D). All cells appeared healthy and did not show clear signs of stress such as changes in cell or nuclear shape or presence of vacuoles. These data indicate that overexpression of mutant HSPB8 does not affect glial cells, suggesting a neuron-specific toxicity.

To check whether other neuronal cell types were affected in the same way as motor neurons, we isolated sensory neurons from DRGs and cortical neurons from brain tissue of C57BL6 mouse E13 and E15 embryos, respectively. Purity of the cultures was confirmed by immunostaining with neuron-specific beta III tubulin antibody. Primary neurons were transduced with WT-HSPB8 or mutant (K141N and K141E)-HSPB8-GFP fusion constructs, yielding similar expression levels of both WT and mutant proteins (Supplementary Material, Fig. S1C and D).

The majority of the primary sensory neurons expressing mutant K141N-HSPB8 appeared healthy and morphologically similar to WT-HSPB8 or native GFP expressing sensory neurons (Fig. 4A–C). However, beaded neurites were observed in ∼10% of the mutant K141E-HSPB8 expressing sensory neuronal cells, similarly to what we saw before in motor neurons, though to a lower extent (10 versus 80%) (Fig. 4D) (GFP = 0.0 ± 0.0%, $n = 655$; WT-HSPB8-GFP = 0.0 ± 0.0%, $n = 436$; K141N-GFP = 0.5 ± 0.0%, $n = 578$, P-value = 0.221 and K141E-GFP = 9.7 ± 1.9%, $n = 660$, P-value = 0.000) (Fig. 4E).

Interestingly, cortical neurons expressing both mutant HSPB8 proteins were morphologically normal and indistinguishable from WT-HSPB8 or native GFP expressing neurons (Fig. 5A–D). Over 100 cortical neurons expressing either mutant or WT-HSPB8-GFP constructs were examined and no beaded or shortened neurites were observed. These results clearly show that the cellular defects caused by mutations in HSPB8 are manifested in neuronal cells originating from the peripheral nervous system and not in cells from the central nervous system. Furthermore, they appear much more pronounced in motor neurons compared with sensory neurons.

Motor neurons expressing mutant HSPB8 show neurite degeneration without signs of apoptosis in the cell body

Neuronal cell death via apoptosis is often linked to neurodegenerative diseases (18). Therefore, we evaluated whether apoptotic pathways were activated in motor neurons expressing mutant HSPB8 by using a TUNEL assay. This assay is used for the detection and quantification of apoptosis at single cell level, based on labeling of DNA strand breaks.

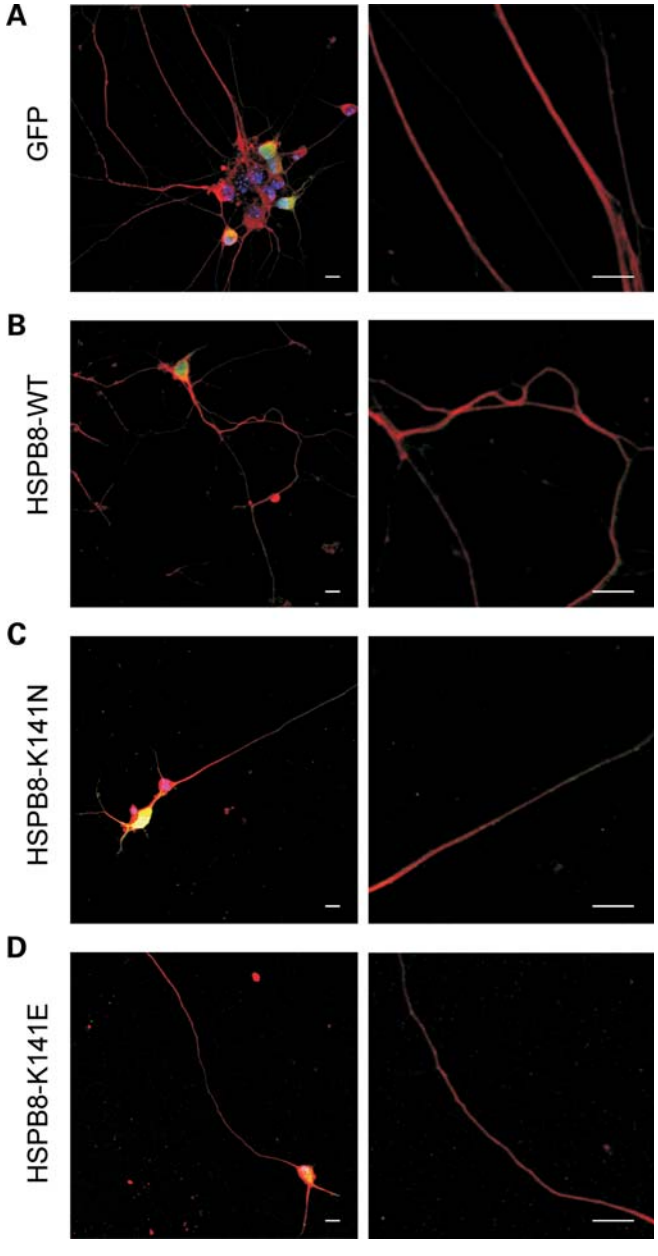

Figure 5. Cortical neurons expressing mutant HSPB8 do not show neurite abnormalities. Mouse cortical neurons were transduced with pLenti-GFP (**A**), pLenti-WT-HSPB8-GFP (**B**), mutant pLenti-K141N-HSPB8-GFP (**C**) or pLenti-K141E-HSPB8-GFP (**D**) constructs at DIV3 and immunostained with β-III tubulin at DIV7. Merged confocal micrographs of GFP (green) and β-III tubulin (red) are shown. Expression of the different HSPB8 constructs did not result in abnormal neurite formation. Scale bar = 10 μm.

Etoposide treatment was used as a positive control to induce apoptosis in transduced motor neuron cultures (Fig. 6A). An additional internal positive control for the TUNEL staining was provided by the TUNEL-positive nuclei of dead cells always present in primary cultures (arrow heads in Fig. 6).

As expected, motor neurons expressing WT-HSPB8 protein or GFP constructs were TUNEL negative (Fig. 6B and C). Interestingly, motor neurons expressing mutant HSPB8-K141E or HSPB8-K141N protein were equally TUNEL negative, despite the presence of spheroids and shortened neurites (Fig. 6D and E). Over 100 motor neurons expressing either mutant or WT-HSPB8-GFP constructs were examined and no link could be observed between TUNEL-positive cells and mutant HSPB8 expression. Similarly to motor neurons, neither the sensory nor the cortical neurons expressing WT-HSPB8 or mutant HSPB8 protein were TUNEL positive (Supplementary Material, Figs S2 and S3). Identical results were also observed in glial cells expressing HSPB8 (data not shown).

To further exclude that expression of mutant HSPB8 induces apoptosis, we investigated the activation status of apoptotic markers in primary neurons, glial cells and in a neuronal cell line (SH-SY5Y) stably expressing WT or mutant HSPB8. Three well-established apoptotic markers were evaluated: cleaved caspase 3, cleaved caspase 9 and cleaved poly (ADP-ribose) polymerase (PARP) (19,20). Confirming our results obtained with the TUNEL assay, no evidence of accumulation of these apoptotic markers was detected in primary motor neurons despite the clear neurite degeneration phenotype (Fig. 7B). Similarly, no accumulation of apoptotic markers could be detected in glial cells or in the stably expressing SH-SY5Y cells (Fig. 7A–C). These results strongly indicate that the degeneration caused by mutant HSPB8 is neurite specific and does not activate classical apoptotic pathways.

DISCUSSION

An increasing number of ubiquitously expressed genes have been identified as the genetic culprits of a number of inherited peripheral neuropathies (7). Mutations in the small heat shock proteins HSPB8 (HSP22) have been associated with distal HMN and CMT2 (1). The HSPB8 mutations target a hot-spot Lysine residue at position 141 located in the predicted β7 strand of the conserved α-crystallin domain (21). In distal HMN patients, the disease phenotype presents first with paresis of the extensor muscles of the feet, which rapidly progresses to paralysis and weakness of all distal muscles of the lower extremities within 5 years (7,22,23).

How defects in HSPB8 basic functions could result in motor neuron degeneration while leaving other tissues unaffected remains an enigma. Changes in the protein structure of mutant HSPB8 could result in inefficient quality control activities (24,25). This, in turn, could reduce the maintenance of peripheral neuron homeostasis plausibly blocking axonal transport, which is a common feature in peripheral neuropathy. To shed some light on this mystery, we studied the effects of HSPB8 mutant proteins in primary neuronal culture.

The HSPB8 protein is ubiquitously expressed in most cell types with particularly high levels in muscle and nervous tissue (5,26). We studied the effect of mutant HSPB8 proteins in primary glial cells and in three different neuronal cell types: motor neurons, sensory neurons and cortical neurons. Our studies demonstrated that lentiviral transduction of mutant HSPB8 promoted the selective degeneration of motor neuron neurites while leaving other cell types mostly unaffected.

Motor neurons expressing the K141N-HSPB8 mutation showed a phenotype consisting of reduced or shortened neur-

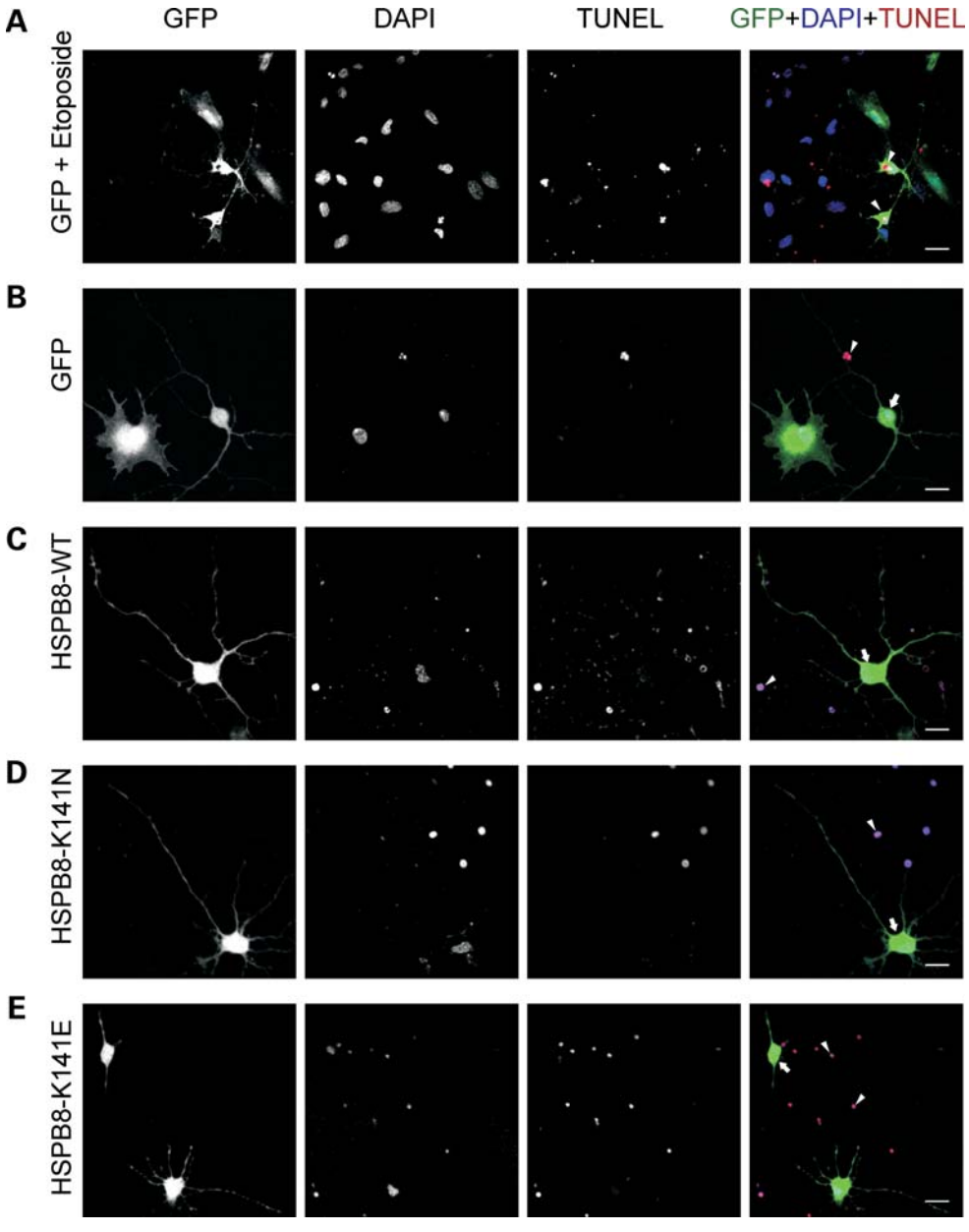

Figure 6. Apoptosis analysis of motor neurons expressing mutant HSPB8. Rat motor neurons were transduced with pLenti-GFP, pLenti-WT-HSPB8-GFP or mutant pLenti-K141N/K141E-HSPB8-GFP constructs at DIV3 and analyzed for the activation of apoptosis at DIV7 with the TUNEL assay which detects DNA breaks in the nuclei of apoptotic cells. Confocal micrographs are shown of GFP expression (green in merge), nuclei of all cells (apoptotic and non-apoptotic, DAPI, blue in merge) and nuclei of apoptotic cells (TUNEL, red in merge). Treating the motor neuron cultures with 50 μM etoposide for 2 h was used as a positive control for cell death activation (**A**). Expression of the different constructs did not lead to detectable TUNEL staining (**B**–**E**). An additional internal positive control was provided by the TUNEL-positive nuclei resulting from dead cells always present in the primary cultures (arrowheads). Motor neurons expressing mutant K141E-HSPB8-GFP exhibit beaded or shortened neurites, but do not have TUNEL-positive nuclei (E). Arrowheads indicate TUNEL-positive cells and arrows indicate GFP or HSPB8-positive TUNEL-negative cells. Scale bar = 10 μm.

ites in ~80% of K141N expressing motor neurons. Motor neurons expressing the K141E-HSPB8 mutation showed a more pronounced phenotype consisting of shortened neurites as well as neurites that were disfigured by a series of regularly spaced, coarse dilatations, which we refer to as spheroids or beaded neurites. Since we did not follow particular neurites over time, we cannot claim at this stage whether the phenotype of the shortened neurites is caused by retraction or by lack of growth. However, since we also observed the presence of beaded neurites, which is a well-established marker of axonal degeneration (16), we consider our present results indicative of retraction rather than a lack of outgrowth. Interestingly, DRG sensory neurons expressing the K141N-HSPB8 did not exhibited any obvious morphological phenotype, whereas the K141E-HSPB8 mutation showed very mild neurite degeneration with only 10% of the neurites being affected. Cortical neurons and glial cells expressing mutant HSPB8 did not exhibit any obvious morphological phenotype.

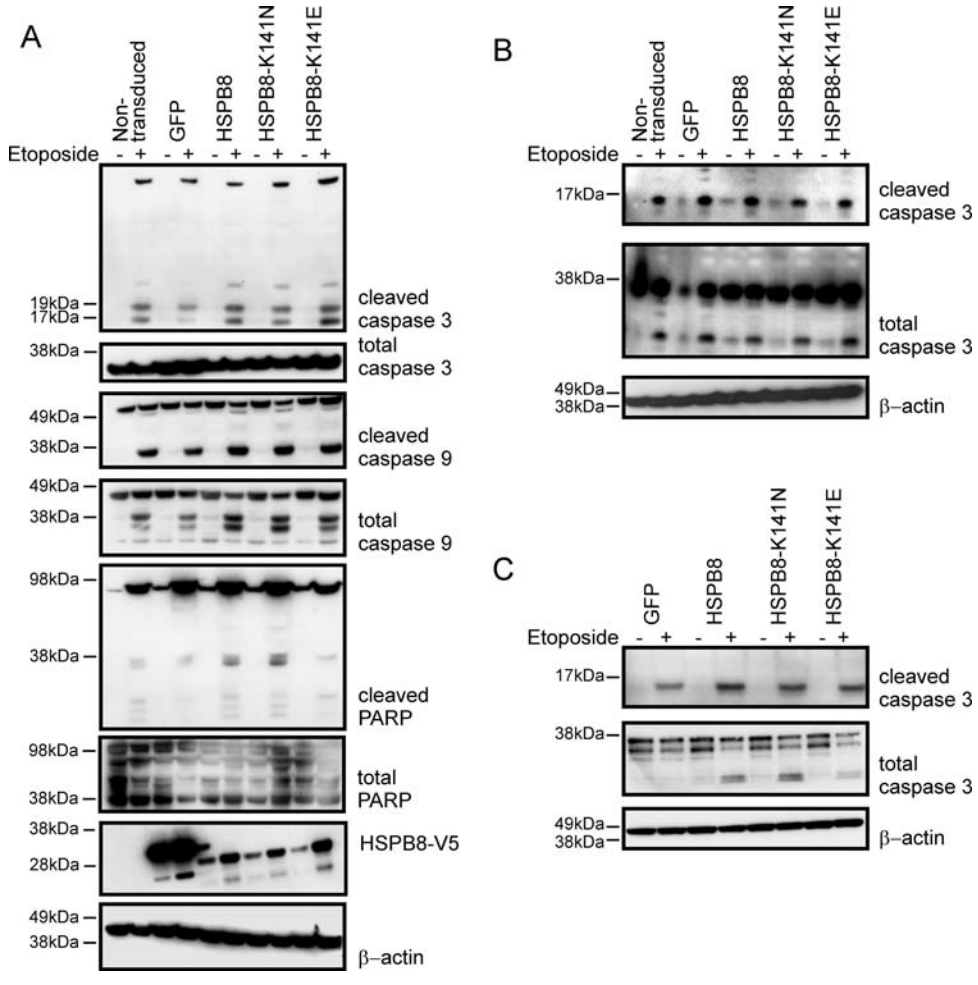

Figure 7. Expression of mutant HSPB8 does not result in increased activation of apoptosis in different neuronal and non-neuronal cell types. Activation of enzymes implicated in initiation and execution of apoptosis was examined by western blot of cleaved (17, 19 kDa) and total caspase 3 (35 kDa), cleaved (35, 37 kDa) and total caspase 9 (47 kDa) and cleaved (89 kDa) and total PARP (116 kDa) in different cell types. Stimulation with etoposide (4 h in 50 μM) was used as a positive control for apoptosis activation in the human neuronal cell line SH-SY5Y stably expressing GFP, WT-HSPB8-V5 or mutant K141N/K141E-HSPB8-V5 constructs (**A**), in rat primary motor neurons (**B**) and in rat primary glial cells (**C**) transduced with pLenti-GFP, pLenti-WT-HSPB8-GFP or mutant pLenti-K141N/K141E-HSPB8-GFP constructs. Expression of mutant HSPB8 did not result in increased basal levels or in increased activation after etoposide treatment of the markers for apoptosis. Normalization was performed with β-actin.

This indicates that although the brunt of the injury in motor neuropathies falls on the motor neurons there might also be some minor sensory involvement. These observations are compatible with the clinical findings in distal HMN patients in whom motor nerves are more affected than sensory nerves and no cognitive impairment is found. The clinical presentation of both mutations is not overtly different. Patients bearing the K141N or K141E mutations have been associated with either a predominant motor neuropathy with very mild sensory disturbance (distal HMN type II) or a motor and sensory neuropathy (CMT2L) (7–9). *In silico* programs predicting the pathogenicity of mutation could not predict which mutation is severer; it is likely that the disease in these CMT2 families represents a phenotypic variant of the clinical continuum associated with α-crystallin mutations and that a diagnosis of CMT2 rather than distal HMN was prompted by the presence of more pronounced sensory symptoms (27).

However, while our experimental findings appear to support the clinical findings, we cannot deny the fact that motor neurons in culture appear to be much more vulnerable to environmental stress than the other neuronal cells used in this study. Therefore, we cannot exclude the possibility that the motor neuron-specific phenotype we observed reflects the sensitivity of motor neurons in culture rather than that it recapitulates the disease phenotype. Still, we rarely observed degenerated or shortened neurites in WT-HSPB8 expressing motor neurons, clearly showing the toxicity of HSPB8 mutations to motor neurons.

Though a lot is known about motor neuron function in health and disease, there are still no obvious explanations found for the selective motor neuron vulnerability. A characteristic that separates peripheral nerves from other cells is their peculiar morphology (28). The axons of lower motor neurons (up to 1 m long) run in peripheral nerves and terminate at neuromuscular junctions of innervated muscles. This size demands a high metabolic load and precise connectivity on the normal sized cell body, and may be particularly vulnerable to free radical-mediated injury (17,28,29). Although

motor and sensory neurons share a similar morphology, the mechanisms that cause more severe motor neuron—and to a lesser extent—sensory neuron degeneration, is unknown. Several susceptibility factors might be implicated in motor neuron cell death specificity, including: differences in subtype transmitter metabolism, variations in subtype connectivity, the size of the neuron, variations in glial environment homeostasis, availability of blood supply in specific regions, environmental toxins, differences in mitochondrial metabolism and sensitivity to oxidative stress, neurofilament alterations, and differences in gene expression. These susceptibility factors may increase the vulnerability of motor neuron viability during disease.

Apoptotic cell death is the predominant form of cell loss in many neurodegenerative diseases (18). We studied the significance of HSPB8 mediated cell death in primary glial cells and neuronal cultures. Surprisingly, no signs of apoptosis could be detected in any of the cells tested upon expression of either WT or mutant HSPB8. Even motor neurons that showed strong features of neurite degeneration appeared to be TUNEL negative, showing that the two phenomena occur independently, at least at this stage. In support of our data, it has been reported before that axon degeneration is an independent process, which often precedes the death of the cell body (30) and that axonal pathology rather than neuronal cell death could be the problem in peripheral neuropathies (16,30,31). Nonetheless, we cannot exclude the possibility that over prolonged time periods subtle neurotoxic mutations in the patients could result in loss of ventral horn motor neurons and could contribute to the ultimate progression of the disease.

It is known that axonal spheroids (beaded neurites) and end bulbs (shortened neurites) may develop after focal blockages of axonal transport. In support of this theory, we found that motor neurons expressing mutant HSPB8 showed approximately a 13% increase in APP accumulation in neurites compared with WT-HSPB8 neurites. Neurite degeneration is often accompanied by minor swelling of axons (varicosities, less than 10 μm) that later increase in size (10–50 μm) to form axonal spheroids (16), very similar to what we observed. Spheroids are often filled with a disorganized cytoskeleton and organelles, and many stain positively for APP (16). As the spheroids grow, axonal transport may become increasingly impaired, and this sequence of events could eventually trigger a phenomenon similar to Wallerian degeneration of the distal axon, resulting in an end bulb (16). Our data further support the hypothesis that dying back axon degeneration pathologies, as in peripheral neuropathies, seem to bear strong similarities to Wallerian-like degeneration in that both show blockages in axonal transport and distal neurite degeneration without any link to apoptosis (16,31–34).

In conclusion, we demonstrated that mutant HSPB8 significantly affects motor neurons, and mildly affects sensory neurons while leaving cortical neurons and glial cells unaffected. Our data support the clinical descriptions of distal HMN type II implying that mutant HSPB8 could cause defects in preserving specifically motor neuron axons. Our future experiments will be focused on elucidating the precise mechanism how mutant HSPB8 induces neurite degeneration using disease models, with the goal of ameliorating the disease phenotype.

MATERIALS AND METHODS

All animal experiments were approved by the University of Antwerp ethics committee and conducted according to the guidelines of the Federation of European Laboratory Animal Science Associations (FELASA).

Isolation of primary cell cultures

Motor neuron-enriched spinal cultures were maintained as described previously (35,36). Briefly, spinal cords were dissected from E13/E14-day-old Wistar rat embryos. The spinal cords were stripped of meninges and DRG and separated into ventral and dorsal halves. The ventral cords were cut into pieces and dissociated by trypsin treatment and by trituration. Culturing the cells at this stage without any further purification generates a mixed culture, consisting of motor neurons, interneurons and glial cells (data not shown). A motor neuron-enriched neuronal population was obtained by centrifugation on a 6.2% iodixanol OptiPrep cushion separating the glial cells and smaller neurons from the larger motor neurons. In this study, we used monocultures which were prepared by seeding motor neuron or glial cells on 1.5 μg/ml poly-L-ornithine or 500 μg/ml poly-L-lysine and 3 μg/ml laminin (Sigma) coated cover glasses or culture dishes. Motor neurons were allowed to recover for 3 days in complete neurobasal medium (NB) supplemented with 2% B27, 4g/L D-glucose, 2 mM L-glutamine and 50 ng/ml nerve growth factor, 100 μg/ml penicillin–streptomycin and 2% fetal calf serum (FCS) before transduction. Glial cells were grown in L15 medium supplemented with 3.6 mg/ml D-glucose, 1% glutamax and 100 μg/ml penicillin–streptomycin, 0.2% sodium bicarbonate and 10% FCS. Since the motor neuron monoculture was sensitive to environmental stress, we did not include the mitotic inhibitor 5-fluoro-2′-deoxyuridine and uridine (FUDR, Sigma) in the culture medium to reduce the number of proliferating cells. Neurofilament heavy antibody SMI32 and the specialized morphology of motor neurons [neuronal cells with large pyramidal soma (diameter > 25 μm) which have more than two neurites] were used to discriminate motor neurons from other cells types during quantification of all experiments.

Sensory neurons were isolated from DRGs from E13 C57BL6 mouse embryos as described previously (37). Briefly, embryos were isolated from the uterine horns of pregnant mice. The spinal cords were dissected and DRGs were carefully removed. DRGs were enzymatically and mechanically dissociated and cells were seeded on 1 mg/ml poly-L-lysine and 3 μg/ml laminin coated culture dishes or cover glasses, and maintained in complete NB medium. During the first days of culturing, a co-culture of sensory neurons, fibroblasts and a small number of satellite cells were observed. To obtain pure sensory neuron cultures, cycling every 2 days between the complete NB medium and the complete NB medium enriched with 1% (v/v) FUDR (final 10 μM FdU and 10 μM uridine) was necessary to kill rapidly dividing cells.

To obtain cortical neuron cultures, C57BL6 mouse E15 embryos were removed from the placenta and placed in a Petri dish containing Hank's Buffered Salt Solution and Hepes. Brains were dissected and the meninges were removed. Mixed cultures of cortical neurons were made from trypsinized brains

as previously reported (38). Neurons were resuspended by careful trituration and plated in minimum essential medium (MEM) supplemented with 10% heat-inactivated horse serum. Neurons were grown on cell culture dishes and cover glasses that were precoated with 1 mg/ml poly-L-lysine and 3 μg/ml laminin. Cortical neurons were allowed to attach in MEM medium for 24 h and subsequently grown in complete NB medium.

Lentiviral transduction

Transduction was performed using the pLenti6/V5-DEST vectors (Invitrogen) containing the human CMV immediate early promoter. The destination vectors are adapted for use with the Gateway® Technology, and are designed to allow high-level expression of recombinant fusion proteins in dividing and non-dividing mammalian cells using a replication-incompetent lentivirus. WT and mutant HSPB8-GFP fusion constructs were PCR amplified with proof reading enzymes and gateway entry and expression clones were created in the pLenti6-DEST vectors. All constructs were sequence verified. Lentivirus encoding HSPB8-GFP WT and mutant fusion constructs were produced in HEK293T cells by cotransfection of 10 μg of pLenti-HSPB8 expression constructs together with 3 μg of pMD2-VSV and 6.5 μg of pCMV-R8.91 viral packaging vectors for lentivirus using the calcium phosphate transfection method. After 8 h of transfection, the calcium transfection medium was removed, the cells were washed with PBS and replaced with medium containing 10 mM sodium butyrate to enhance promoter activity. The next day the medium was replaced with 8 ml complete NB medium and lentivirus was produced for 24 h. The produced lentivirus was harvested by filtering the supernatant of the HEK293T cells. We used 1000 lentiviral particles per cell to transduce the primary cells seeded on culture dishes or cover glasses. GFP fluorescence was visible in transduced cells after 3–4 days. The transduction efficiency of the primary cells was over 70%.

Generation of SH-SY5Y stable cell lines expressing HSPB8

To generate stable SH-SY5Y cell lines, we made constructs encoding different HSPB8 mutations or EGFP using the Gateway recombination system (Invitrogen). Using primers containing the attB recombination sites, open reading frames (ORFs) from HSPB8 WT, K141N and K141E were amplified from constructs described elsewhere (5). The EGFP cassette was amplified from pEGFP-N1 (Clontech). The PCR products containing the ORFs flanked by the attB recombination sites were then recombined into a pDONR221 vector and sequence validated. The validated pDONRs-HSPB8 constructs were then transferred by recombination to the pLENTI6/V5-Dest (Invitrogen) generating constructs with the ORFs C-terminally fused to a V5-tag. Stable cell lines were produced by lentiviral transduction of the neuronal cell line SH-SY5Y, according to the method described by Salmon and Trono (39).

After infection, the cells were selected in MEM media supplemented with 10% FCS, 1% non-essential amino acids, 2 mM glutamine and 100 μg/ml penicillin/streptomycin and blasticidin (3 μg/ml) for 3–4 weeks. The whole population of selected cells was pooled for further experiments. After selection, cells were cultured in MEM medium supplemented with 10% fetal bovine serum and blasticidin (3 μg/ml). Stable cell lines showed similar expression levels of the HSPB8 gene by western blot.

Immunocytochemistry and microscopy experiments

Cells were fixed in 3% paraformaldehyde using standard protocols (5). We tested several established motor neuronal markers including the choline acetyl transferase (ChAT), beta-3 tubulin, the non-phosphorylated neurofilament heavy isoform (SMI32) and 75 kDa low-affinity neurotrophin receptor (p75NTR). We found that SMI32 and beta-3 tubulin specifically labeled neuronal cells and gave the best results in our hands. SMI32 neurofilament antibody is a well-established motor neuron marker (40,41).

Immunostaining was performed with the following glial or neuronal antibodies and dilutions: GFAP (1/1000, Chemicon International), Schwann cell/oligodendrocyte marker 2′,3′-cyclic nucleotide 3′-phosphodiesterase (CNPase, 1/200, Abcam), non-phosphorylated epitope in neurofilament H (SMI32, 1/1000, Sternberger monoclonals), neuron specific beta III tubulin (β-III tubulin, 1/500, Abcam) and APP antibody (APPC20/2, I/1000, custom made by Sigma). Alexa Fluor 594 antibodies (Invitrogen) were used as secondary antibodies for fluorescence detection. Dapi or Hoechst 33342 (1/20000, Invitrogen) was used to stain the nucleus. Cells were microscopically examined and images were acquired by the use of different (confocal) microscopes: Zeiss Axiovert 200 with apotome technology (60X 1.4 NA-objective; GFP detection: BP 500/20, FT 515, BP 535/30; AF555, AF594 and TUNEL detection: BP 545/25, FT 570, BP 605/70; DAPI detection: G 365, FT 395, BP 445/50), Zeiss LSM700 (60X 1.4 NA-objective; 405, 488, 514 nm solid state lasers and variable secondary dichroic technology) and Zeiss LSM510 (60X 1.4 NA-objective) confocal microscope equipped with an Argon (488 nm), two Helium/Neon (543 and 633 nm) and a tunable Titan/sapphire laser (700–1000 nm). Images were processed with the AxioVision, LSM510 or Zen 2008 browser software (Zeiss), ImageJ (42) and CorelDraw (http://www.pcpro.co.uk/reviews/software/158352/coreldraw-graphics-suite-x4).

Detection of DNA strand breaks in cultured cells

To detect apoptotic cell death in individual cells, primary neurons and glial cells were fixed with 3% formaldehyde in PBS and DNA fragmentation in nuclei of cells in apoptosis was stained by use of a TUNEL detection assay. We used the *In Situ* Cell Death Detection Kit (TMR red, Roche) according to the manufacturer's protocol. Briefly, the assay measures and quantifies apoptotic cell death by labeling and detection of DNA strand breaks in individual cells by flow cytometry or fluorescence microscopy. Cells were incubated with the TUNEL reaction mixture containing TdT and TMR-dUTP. During an incubation step, TdT catalyzes the attachment of TMR-dUTP to free 3′OH ends in the DNA.

Western blotting

Cells were lysed in NP40 lysis buffer (250 mM NaCl, 1 mM EDTA, 20 mM HEPES pH 7.9, 1% NP40, 20 mM b-glycerophosphate, 10 mM Sodium fluoride, 4 mM Sodium

orthovanadate, 400 μg/ml Sodium-pyrophosphate, 2 mM DDT) supplemented with protease inhibitor cocktail (Roche) for 20 min on ice and cleared by centrifugation. When the number of neurons was limited, we directly lysed cells on plate with 1x NuPage sample buffer (Invitrogen, 5X NuPage sample buffer = 250 mM Tris–HCl pH 6.8, 10% SDS, 30% Glycerol, 0.02% bromophenol blue, supplemented with 100 mM DTT), followed by sonication. Cell extracts were boiled for 5 min and equal concentrations of cell lysates were resolved on a SDS-NuPage gel. The gel was transferred to nitrocellulose membrane and processed for western blotting as described previously (5,43). For analysis of apoptosis, we used: cleaved caspase 3, total caspase 3, cleaved caspase 9, total caspase 9, cleaved PARP and total PARP (all antibodies were obtained from Cell Signalling and used at 1/1000 dilution). For the analysis of protein expression, we used commercial available monoclonal HSPB8 antibodies: clone 2H5 (Abcam, cat. no. ab15896, no longer commercially available, 1/2000), GFP antibody JL8 (Clontech, 1/5000), anti-V5 antibody (Invitrogen, 1/5000) and anti-β-Actin (Sigma, 1/5000).

Quantification of neurite degeneration and statistical analysis

Data showing incidence of events in neuronal cells (neurite degeneration, reduction of neurite length, strong APP accumulation) were expressed as mean percentages ± standard deviation, after counting multiple random regions from three independent experiments. Cell counts were done blinded and all experiments were repeated independently. Statistical comparison was done by using Student's *t*-test.

Cells were defined to have reduced neurite length if the neurites did not extend a 40× microscopic field of view. For the data presented in Fig. 1F, the number of counted motor neurons is $n = 361$ for GFP, $n = 192$ for HSPB8-WT, $n = 150$ for HSPB8-K141N and $n = 300$ for HSPB8-K141E. In the assay in which the proportion of cells with beaded neurites was counted (Fig. 1G), the number of counted motor neurons was $n = 338$ for GFP, $n = 192$ for HSPB8-WT, $n = 150$ for HSPB8-K141N and $n = 300$ for HSPB8-K141E. In each image mosaiX, the longest neurite length per cell was measured by use of the Zeiss Axiovert 200 measurement tool software and the distribution of neurite lengths was represented as the percentage of neurons with a neurite length longer than the neurite length being measured (abscissa), also referred to as a 'Chang plot' (44). For the presented data in Figure 1H, the number of measured neurites was $n = 74$ for GFP, $n = 61$ for HSPB8-WT, $n = 30$ for HSPB8-K141N and $n = 47$ for HSPB8-K141E. For average neurite number quantification: $n = 248$ for GFP, $n = 219$ for HSPB8-WT, $n = 428$ for HSPB8-K141N and $n = 424$ for HSPB8-K141E (Fig. 1I). The number of counted sensory neurons (beaded neurite phenotype quantification) was $n = 655$ for GFP, $n = 436$ for HSPB8-WT, $n = 578$ for HSPB8-K141N and $n = 660$ for K141E (Fig. 4E). The incidence of APP accumulation was quantified by randomly counting the proportion of cells with and without strong neuritic APP accumulation. The number of counted motor neuron neurites was $n = 994$ for GFP, $n = 971$ for HSPB8-WT, $n = 864$ for HSPB8-K141N and $n = 1029$ for HSPB8-K141E.

SUPPLEMENTARY MATERIAL

Supplementary Material is available at *HMG* online.

ACKNOWLEDGEMENTS

We would like to thank A. Jacobs and W. Scheveneels for help with cloning and cell culture work. We thank L. Svensson, J. Van Daele and D. De Rijck for assistance with confocal microscopy.

Conflict of Interest statement. None declared.

FUNDING

This work was supported by the Methusalem program of the University of Antwerp and by the University of Leuven, the Fund for Scientific Research (FWO-Flanders), the American Muscular Dystrophy Association (MDA), the Medical Foundation Queen Elisabeth (GSKE), the Association Belge contre les Maladies Neuromusculaires (ABMM) and the Interuniversity Attraction Poles program (P6/43) of the Belgian Federal Science Policy Office (BELSPO). J.K. is a recipient of the PhD scholarship of the Interfaculty Council for Development Co-operation of the University of Leuven (IRO). J.I. and S.J. are supported by postdoctoral fellowships of FWO-Flanders, Belgium. W.R. is supported by the E. von Behring Chair for Neuromuscular and Neurodegenerative Disorders. Funding to pay the Open Access Charge was provided by GSKE.

REFERENCES

1. Dierick, I., Irobi, J., De Jonghe, P. and Timmerman, V. (2005) Small heat shock proteins in inherited peripheral neuropathies. *Ann. Med.*, **37**, 413–422.
2. Haslbeck, M., Franzmann, T., Weinfurtner, D. and Buchner, J. (2005) Some like it hot: the structure and function of small heat-shock proteins. *Nat. Struct. Mol. Biol.*, **12**, 842–846.
3. Walter, S. and Buchner, J. (2002) Molecular chaperones—cellular machines for protein folding. *Angew. Chem. Int. Ed Engl.*, **41**, 1098–1113.
4. Tang, B.S., Zhao, G.H., Luo, W., Xia, K., Cai, F., Pan, Q., Zhang, R.X., Zhang, F.F., Liu, X.M., Chen, B. *et al.* (2005) Small heat-shock protein 22 mutated in autosomal dominant Charcot-Marie-Tooth disease type 2L. *Hum. Genet.*, **116**, 222–224.
5. Irobi, J., Van Impe, K., Seeman, P., Jordanova, A., Dierick, I., Verpoorten, N., Michalik, A., De Vriendt, E., Jacobs, A., Van Gerwen, V. *et al.* (2004) Hot-spot residue in small heat-shock protein 22 causes distal motor neuropathy. *Nat. Genet.*, **36**, 597–601.
6. Evgrafov, O.V., Mersiyanova, I., Irobi, J., Van Den Bosch, L., Dierick, I., Leung, C.L., Schagina, O., Verpoorten, N., Van Impe, K., Fedotov, V. *et al.* (2004) Mutant small heat-shock protein 27 causes axonal Charcot-Marie-Tooth disease and distal hereditary motor neuropathy. *Nat. Genet.*, **36**, 602–606.
7. Irobi, J., Dierick, I., Jordanova, A., Claeys, K.G., De Jonghe, P. and Timmerman, V. (2006) Unraveling the genetics of distal hereditary motor neuronopathies. *Neuromolecular Med.*, **8**, 131–146.
8. Harding, A.E. and Thomas, P.K. (1980) Hereditary distal spinal muscular atrophy. A report on 34 cases and a review of the literature. *J. Neurol. Sci.*, **45**, 337–348.
9. Tang, B.S., Luo, W., Xia, K., Xiao, J.F., Jiang, H., Shen, L., Tang, J.G., Zhao, G.H., Cai, F., Pan, Q. *et al.* (2004) A new locus for autosomal dominant Charcot-Marie-Tooth disease type 2 (CMT2L) maps to chromosome 12q24. *Hum. Genet.*, **114**, 527–533.

10. Houlden, H., Laura, M., Wavrant-DeVrieze, F., Blake, J., Wood, N. and Reilly, M.M. (2008) Mutations in the HSP27 (HSPB1) gene cause dominant, recessive, and sporadic distal HMN/CMT type 2. *Neurology*, **71**, 1660–1668.
11. Kijima, K., Numakura, C., Goto, T., Takahashi, T., Otagiri, T., Umetsu, K. and Hayasaka, K. (2005) Small heat shock protein 27 mutation in a Japanese patient with distal hereditary motor neuropathy. *J. Hum. Genet.*, **50**, 473–476.
12. Lazarov, O., Morfini, G.A., Lee, E.B., Farah, M.H., Szodorai, A., Deboer, S.R., Koliatsos, V.E., Kins, S., Lee, V.M., Wong, P.C. *et al.* (2005) Axonal transport, amyloid precursor protein, kinesin-1, and the processing apparatus: revisited. *J. Neurosci.*, **25**, 2386–2395.
13. Salinas, S., Bilsland, L.G. and Schiavo, G. (2008) Molecular landmarks along the axonal route: axonal transport in health and disease. *Curr. Opin. Cell Biol.*, **20**, 445–453.
14. McKenzie, K.J., McLellan, D.R., Gentleman, S.M., Maxwell, W.L., Gennarelli, T.A. and Graham, D.I. (1996) Is beta-APP a marker of axonal damage in short-surviving head injury? *Acta Neuropathol.*, **92**, 608–613.
15. Sherriff, F.E., Bridges, L.R., Gentleman, S.M., Sivaloganathan, S. and Wilson, S. (1994) Markers of axonal injury in post mortem human brain. *Acta Neuropathol.*, **88**, 433–439.
16. Coleman, M. (2005) Axon degeneration mechanisms: commonality amid diversity. *Nat. Rev. Neurosci.*, **6**, 889–898.
17. Gilley, J. and Coleman, M.P. (2010) Endogenous Nmnat2 is an essential survival factor for maintenance of healthy axons. *PLoS Biol.*, **8**, e1000300.
18. Friedlander, R.M. (2003) Apoptosis and caspases in neurodegenerative diseases. *N. Engl. J. Med.*, **348**, 1365–1375.
19. Kroemer, G., Galluzzi, L., Vandenabeele, P., Abrams, J., Alnemri, E.S., Baehrecke, E.H., Blagosklonny, M.V., El-Deiry, W.S., Golstein, P., Green, D.R. *et al.* (2009) Classification of cell death: recommendations of the Nomenclature Committee on Cell Death 2009. *Cell Death Differ.*, **16**, 3–11.
20. Van den Berghe, T., Denecker, G., Brouckaert, G., Vadimovisch, K.D., D'Herde, K. and Vandenabeele, P. (2004) More than one way to die: methods to determine TNF-induced apoptosis and necrosis. *Methods Mol. Med.*, **98**, 101–126.
21. Kasakov, A.S., Bukach, O.V., Seit-Nebi, A.S., Marston, S.B. and Gusev, N.B. (2007) Effect of mutations in the beta5-beta7 loop on the structure and properties of human small heat shock protein HSP22 (HspB8, H11). *FEBS J.*, **274**, 5628–5642.
22. Timmerman, V., Raeymaekers, P., Nelis, E., De Jonghe, P., Muylle, L., Ceuterick, C., Martin, J.J. and Van Broeckhoven, C. (1992) Linkage analysis of distal hereditary motor neuropathy type II (distal HMN II) in a single pedigree. *J. Neurol. Sci.*, **109**, 41–48.
23. Irobi, J., De Jonghe, P. and Timmerman, V. (2004) Molecular genetics of distal hereditary motor neuropathies. *Hum. Mol. Genet.*, **13**, 195–202.
24. Carra, S., Sivilotti, M., Chavez Zobel, A.T., Lambert, H. and Landry, J. (2005) HspB8, a small heat shock protein mutated in human neuromuscular disorders, has in vivo chaperone activity in cultured cells. *Hum. Mol. Genet.*, **14**, 1659–1669.
25. Carra, S., Brunsting, J.F., Lambert, H., Landry, J. and Kampinga, H.H. (2009) HspB8 participates in protein quality control by a non-chaperone-like mechanism that requires eIF2 alpha phosphorylation. *J. Biol. Chem.*, **284**, 5523–5532.
26. Benndorf, R., Sun, X., Gilmont, R.R., Biederman, K.J., Molloy, M.P., Goodmurphy, C.W., Cheng, H., Andrews, P.C. and Welsh, M.J. (2001) HSP22, a new member of the small heat shock protein superfamily, interacts with mimic of phosphorylated HSP27 ((3D)HSP27). *J. Biol. Chem.*, **276**, 26753–26761.
27. Dierick, I., Baets, J., Irobi, J., Jacobs, A., De Vriendt, E., Deconinck, T., Merlini, L., Van den Bergh, P., Rasic, V.M., Robberecht, W. *et al.* (2008) Relative contribution of mutations in genes for autosomal dominant distal hereditary motor neuropathies: a genotype–phenotype correlation study. *Brain*, **131**, 1217–1227.
28. Bruijn, L.I., Miller, T.M. and Cleveland, D.W. (2004) Unraveling the mechanisms involved in motor neuron degeneration in ALS. *Annu. Rev. Neurosci.*, **27**, 723–749.
29. Trounce, I., Feeney, S. and Byrne, E. (2003) Pathoetiology of motor neuron disease: new insights from genetics and animal models. *J. Clin. Neurosci.*, **10**, 293–296.
30. Raff, M.C., Whitmore, A.V. and Finn, J.T. (2002) Axonal self-destruction and neurodegeneration. *Science*, **296**, 868–871.
31. Mack, T.G., Reiner, M., Beirowski, B., Mi, W., Emanuelli, M., Wagner, D., Thomson, D., Gillingwater, T., Court, F., Conforti, L. *et al.* (2001) Wallerian degeneration of injured axons and synapses is delayed by a Ube4b/Nmnat chimeric gene. *Nat. Neurosci.*, **4**, 1199–1206.
32. Cavanagh, J.B. (1979) The 'dying back' process. A common denominator in many naturally occurring and toxic neuropathies. *Arch. Pathol. Lab Med.*, **103**, 659–664.
33. Ferri, A., Sanes, J.R., Coleman, M.P., Cunningham, J.M. and Kato, A.C. (2003) Inhibiting axon degeneration and synapse loss attenuates apoptosis and disease progression in a mouse model of motoneuron disease. *Curr. Biol.*, **13**, 669–673.
34. Samsam, M., Mi, W., Wessig, C., Zielasek, J., Toyka, K.V., Coleman, M.P. and Martini, R. (2003) The Wlds mutation delays robust loss of motor and sensory axons in a genetic model for myelin-related axonopathy. *J. Neurosci.*, **23**, 2833–2839.
35. Vandenberghe, W., Van Den Bosch, L. and Robberecht, W. (1998) Glial cells potentiate kainate-induced neuronal death in a motoneuron-enriched spinal coculture system. *Brain Res.*, **807**, 1–10.
36. Van Damme, P., Bogaert, E., Dewil, M., Hersmus, N., Kiraly, D., Scheveneels, W., Bockx, I., Braeken, D., Verpoorten, N., Verhoeven, K. *et al.* (2007) Astrocytes regulate GluR2 expression in motor neurons and their vulnerability to excitotoxicity. *Proc. Natl Acad. Sci. USA*, **104**, 14825–14830.
37. Taveggia, C., Zanazzi, G., Petrylak, A., Yano, H., Rosenbluth, J., Einheber, S., Xu, X., Esper, R.M., Loeb, J.A., Shrager, P. *et al.* (2005) Neuregulin-1 type III determines the ensheathment fate of axons. *Neuron*, **47**, 681–694.
38. Cupers, P., Orlans, I., Craessaerts, K., Annaert, W. and De Strooper, B. (2001) The amyloid precursor protein (APP)-cytoplasmic fragment generated by gamma-secretase is rapidly degraded but distributes partially in a nuclear fraction of neurones in culture. *J. Neurochem.*, **78**, 1168–1178.
39. Salmon, P. and Trono, D. (2006) Production and titration of lentiviral vectors. *Curr. Protoc. Neurosci.*, **Chapter 4**, Unit.12.10.
40. Ishiyama, T., Okada, R., Nishibe, H., Mitsumoto, H. and Nakayama, C. (2004) Riluzole slows the progression of neuromuscular dysfunction in the wobbler mouse motor neuron disease. *Brain Res.*, **1019**, 226–236.
41. Urushitani, M., Shimohama, S., Kihara, T., Sawada, H., Akaike, A., Ibi, M., Inoue, R., Kitamura, Y., Taniguchi, T. and Kimura, J. (1998) Mechanism of selective motor neuronal death after exposure of spinal cord to glutamate: involvement of glutamate-induced nitric oxide in motor neuron toxicity and nonmotor neuron protection. *Ann. Neurol.*, **44**, 796–807.
42. Collins, T.J. (2007) ImageJ for microscopy. *Biotechniques*, **43**, 25–30.
43. Dierick, I., Irobi, J., Janssens, S., Theuns, J., Lemmens, R., Jacobs, A., Corsmit, E., Hersmus, N., Van Den Bosch, L., Robberecht, W. *et al.* (2007) Genetic variant in the HSPB1 promoter region impairs the HSP27 stress response. *Hum. Mutat.*, **28**, 830–841.
44. Chang, S., Rathjen, F.G. and Raper, J.A. (1987) Extension of neurites on axons is impaired by antibodies against specific neural cell surface glycoproteins. *J. Cell Biol.*, **104**, 355–362.